Solid Freeform Fabrication 2016: Proceedings of the 27th Annual International Solid Freeform Fabrication Symposium – An Additive Manufacturing Conference
Reviewed Paper

Real Time Monitoring of Exposure Controlled Projection Lithography with Time-varying Scanning Points

Changxuan Zhao, Amit S. Jariwala, David W. Rosen

G.W.W. School of Mechanical Engineering, Georgia Institute of Technology,
813 Ferst Drive NW, Atlanta, GA 30332-040, USA

Abstract

Exposure Controlled Projection Lithography (ECPL) is a stereolithographic process in which photopolymer resin is used to fabricate lens shaped features. During this process, a dynamic mask projects radiation patterns through a transparent substrate onto the photopolymer resin to grow features from the substrate surface. We present a novel method to monitor the photopolymerization process in real-time with higher spatial resolution in a plane perpendicular to the polymerization growth. A Spatial Light Modulator (SLM) was incorporated into our Interferometric Cure Monitoring (ICM) system, which periodically moves the positions of the scanning points onto the curing area to estimate the cured part height. This time-varying scanning strategy avoids interference caused by points too close to one another and enables higher spatial resolution than fixed scan patterns. This time-varying multi-point monitoring approach is experimentally validated to measure the cured part height and the lateral dimensions of the cured part at the substrate level.

1.Introduction

Exposure Controlled Projection Lithography (ECPL) is a stereolithographic process in which 3D features are fabricated by radiating UV beam with controlled profile patterns onto the photopolymer resin. Lithography processes traditionally use a scanning curing laser with a bath of photopolymer resin to progressively build the 3D features layer by layer. In contrast, Limaye & Rosen[1], Sun et al[2], Chatwin[3], Monneret et al. [4], Jariwala et al. [5], and Zheng et al. [6] investigated building 3D features with dynamic masks which control the radiating patterns of the exposure light source onto photopolymer resins instead of 1D curing laser scanning process. The ECPL system controls the curing light source with dynamic masks and projects this curing source into the resin chamber. The ECPL process differs from the other mask projection processes in that the radiation pattern is projected upwards through a transparent substrate into the resin bath where the features are cured on the transparent substrate. Jariwala et al. [7] [8] proposed an ECPL process planning method which utilizes chemical photopolymerization models of resin to estimate the cured part height. The Interferometric Curing Monitoring (ICM) system was then proposed by Schwerzel et al. [9] to improve the accuracy of 3D feature fabrication. This paper provides a time-varying scanning method using the ICM system to monitor the 1D lateral dimension and height distribution of the cured part during the photopolymerization process. This method has the capability to increase the lateral resolution of the measurement without making substantial improvement to the experimental setup. Experimental results are presented to validate this method.

2.System Overview

2.1 ECPL System

A schematic of the ICM system and the ECPL system is shown in Figure 1. The ICM system includes part (1) to (8), and the ECPL system includes part (9) to (12). During the curing process, the curing light from the UV source passes through the dynamic mask generator (DMD) which forms the curing light beam with its cross-section profile being controlled. The projection system focuses the light onto the resin chamber, and the light passes through the bottom transparent substrate of the resin chamber into the photopolymer resin to begin the curing process. The dynamic mask and exposure time determine the 3D dimensions of the part.

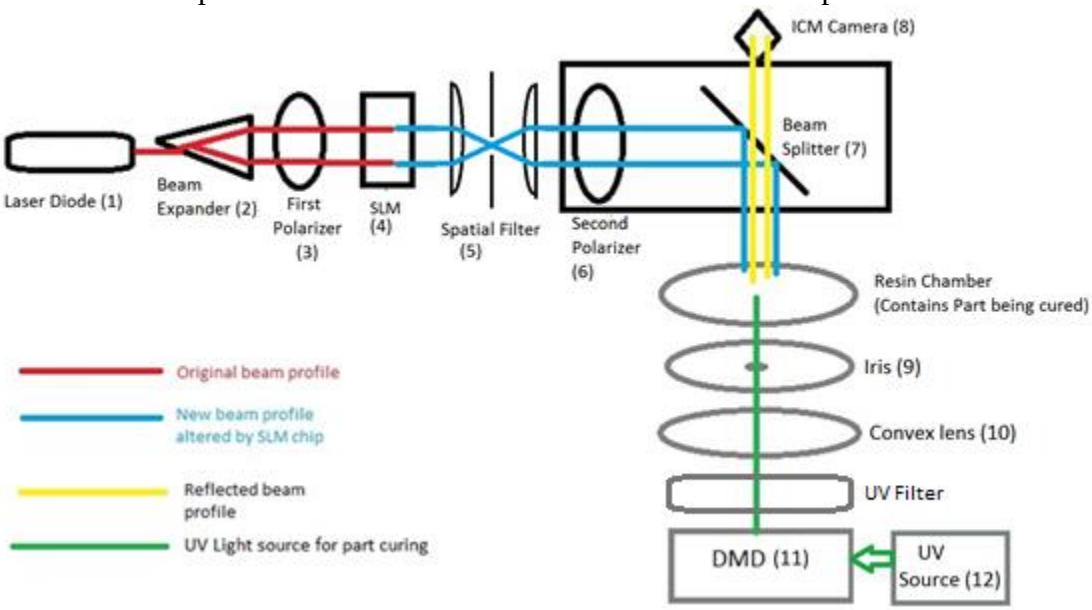

Figure 1. Schematic of ECPL system and ICM system

Radiation Source:

Refer to part (12) in Figure 1, the radiation source used was an Omnicure S2000 UV spot curing system produced by Lumen Dynamics. This radiation source produces UV radiation at wavelength centered at 365 nm. This wavelength was selected to initiate crosslinking in the photopolymer. The resulting beam was introduced into the DMD through a 7 mm optic fiber which guide the light.

Dynamic Mask Generator:

Refer to part (11) in Figure 1, the dynamic mask generator consisted of a Digital Light Innovations' CEL5500 Light Engine. This is a Digital Micromirror Device (DMD) that consists of an array of micro-mirrors. The DMD was controlled as a secondary computer monitor using Microsoft PowerPoint software. The figures displayed by PowerPoint were converted into grayscale information and were sent to the DMD. The DMD then projects the corresponding grayscale radiation upwards to the substrate of the resin chamber.

Projection System:

The projection system consisted of an FB360 bandpass filter, a LA1255 convex lens (part (10) in Figure 1) (25 mm diameter and 50 mm focal length) and an SM1D12 Iris (part (9) in Figure 1) from ThorLabs, Inc. The bandpass filter could filter out the radiation source at wavelength other

than 340-370 nm. The iris could open a pinhole with diameter ranging from 0.8-12 mm. This projection system is used to sharpen the acutance of the dynamic mask and reduce the noise from radiation at wavelength other than the curing wavelength.

Resin Chamber:

The resin chamber consisted of two glass slides separated by spacers of known thickness. The photopolymer resin was loaded between the two glass slides. The photopolymer resin crosslinks inside this resin chamber when exposed to UV radiation.

2.2 ICM System

The Interferometer Cure Monitoring (ICM) system, shown in Figure 2, was based on a Mach-Zehnder interferometer [9]. A coherent laser is directed, through a beam expander, a polarizer, an SLM chip, a spatial filter, another polarizer, and beam splitter, at the resin chamber. Light reflecting off of the top and bottom surface of the resin chamber's two transparent bounding surfaces reflect through the beam splitter and into the camera. Due to the phase difference between the light coming from the top surface and the light coming from the bottom surface an interference pattern is observed by the camera. The ICM working principle will be explained in part 3.

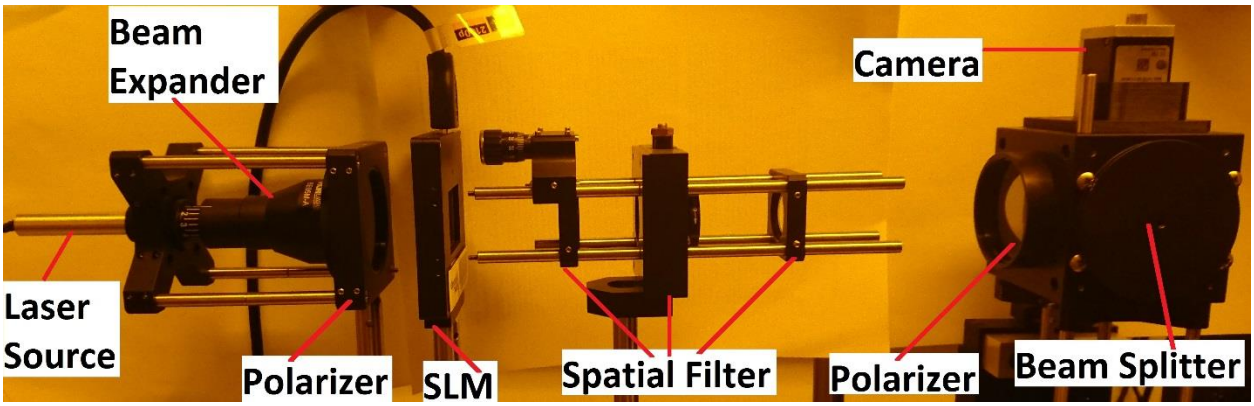

Figure 2. Photograph showing the experimental ICM System Setup

Laser Source

Refer to part (1) in Figure 1, the laser source consisted of a CPS532 Collimated Laser Diode from ThorLabs, Inc. The purpose of this diode was to provide the coherent laser light (at wavelength of 532 nm) required for interferometry.

Beam Expander

Refer to part (2) in Figure 1, the purpose of the beam expander was to expand the narrow beam produced by the laser source such that the light output is capable of selectively scanning at any location inside and near the curing region such that any point around the curing region can be analyzed by the camera.

SLM system

The SLM system was composed of a polarizer (part (3) in Figure 1), an SLM chip (part (4) in Figure 1), the spatial filter (part (5) in Figure 1) which was composed of convex lens-iris-convex lens, and another polarizer (part (6) in Figure 1). The SLM chip with two polarizers on each side of it functions as a movable iris. The spatial filter was added to reduce the diffracted laser patterns which were created when the laser beam passes through the SLM chip. The SLM system has two

functions: to reduce the radius of the laser profile from a circle with large radius to any shapes that were desired and with smaller dimensions, and to enable moving that small profile in lateral directions parallel to the resin chamber. These two functions are necessary to monitor the photopolymerization process.

Camera

Refer to part (8) in Figure 1, the purpose of the camera was to capture the intensity of laser light reflected back from the resin chamber, across the entire curing area. The intensity profile of the resulting laser light shows the interference patterns. Tracking the interference patterns enables calculating the phase shift caused by change in refractive index of the photopolymer being cured inside the resin chamber.

3. ICM Working Principle

The ICM system utilizes the principles of interferometry to track the changes in refractive index within the resin chamber in real time. As discussed by Schwerzel et al. [9], this change in refractive index bears a monotonic relationship with the height of cured part. The camera records the interferogram produced by the phase difference between the light reflecting from the top surface of the resin chamber and the bottom surface of the resin chamber. The thickness of the resin chamber results in steady state optical path offset which equates to a constant phase shift. The curing process causes the photopolymer resin to increase density as it crosslinks, and this changes the refractive index of the resin in the resin chamber. The cured part height can be expressed as a function of the phase shift which is a function of the optical path. Schwerzel et al. [9] proposed the equation for this phase shift as equation 1:

$$shift = \frac{2*\Delta n*t}{\lambda} \tag{1}$$

where Δn is the change in refractive index of cured resin, t is the thickness of the cured part, and λ is the laser wavelength. A linear relationship was experimentally determined between phase shift and the cured part height [9], which provides the fundamental basis for estimating cured part height based on the phase shift of the interference pattern, captured by the ICM camera. The relationship is determined as equation 2:

$$t = a * \ln(\emptyset) + b \tag{2}$$

where t is the cured part height in micron; ϕ is the total phase shift in radian; a and b are two constant parameters that are needed to be calibrated by experiments.

During the experiment [9], a photosensor was used (in place of the camera shown in Figure 2) to capture the intensities of the light reflected from the resin chamber, as a function of time. The intensities of the light at the same coordinate location along different time steps results into an interferogram. An example of the interferogram is shown in Figure 3 [9].

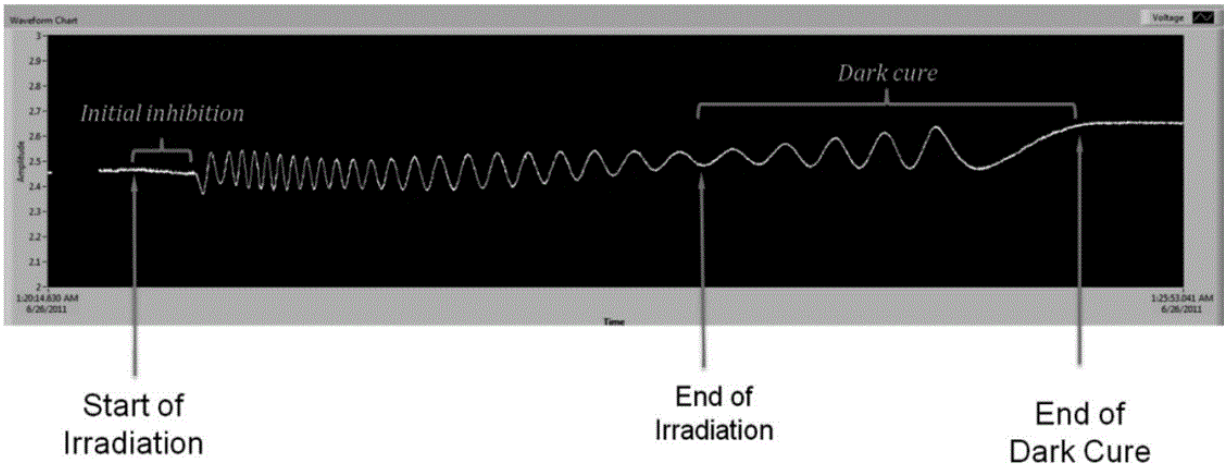

Figure 3. An example of interferogram obtained from the ICM [9]

Figure 3 shows an interferogram obtained while curing a typical sample on the ECPL system. From the interferogram, the different stages of the curing process could be obtained. When the curing started, the intensity started to oscillate with a relatively steady frequency. Indicated by the intensity oscillations with significantly lower frequency, it could be concluded that the UV radiation ended, and the dark curing took place to continue curing the sample without irradiation from the UV source.

4. ICM System Limitations & Research Questions

4.1 System Limitations

The principle of tracking the change in refractive index (as explained in section 3) can be expanded to interrogate across the entire curing region by replacing a single diode photosensor with a camera (as shown in Figure 2). However, recent studies have shown that this method cannot be used to accurately estimate the lateral dimensions of the part being cured. Jones et al. [12] showed that internal reflections within the resin substrate could cause the generation of interferograms (which looks similar to intensity oscillation patterns at the locations inside the curing region), at locations outside the curing region. This inadvertent noise in the signal limits the ability of the ICM system to accurate measure the width of the cured part. Figure 4 shows a schematic of light path of the ICM laser from beam splitter (part (7) in Figure 1) to the ICM camera (part (8) in Figure 1) proposed by Jones et al. [12], which explains the internal diffractions mentioned in this paragraph.

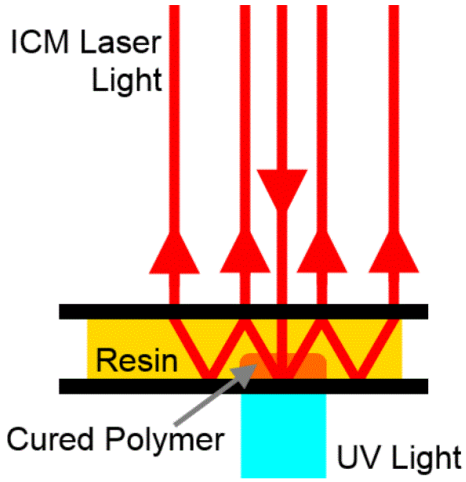

Figure 4. A schematic of the ICM laser light path with internal reflections proposed by Jones et al. [12]

4.2 Research Question and Hypothesis

The research question associated with this paper is how to accurately and efficiently measure the dimensions of the cured part fabricated by the ECPL system. The hypotheses for this research question could be summarized as the following sentences: By using a laser beam with small profile area to scan the interested area instead of bathing the whole curing region with laser beam, a more accurate interferogram at the interested area could be gathered. Thus, the ICM system could detect the edges of the cured part (in the 2D lateral dimensions perpendicular to the cured part height) with more accuracy by scanning a small laser beam among the curing region. In addition, measurements of the width of the cured part with large size, with more efficiency and acceptable accuracy, could be gathered using a matrix of laser beams, in which the neighboring beams do not interfere each other, to scan the curing region.

The SLM could control the ICM laser beam to be several beams for which the neighboring two beams have gap between each other to isolate them. By isolating the neighboring ICM laser beams, the error caused by the internal diffractions could be avoided. In addition, the SLM was able to control these small beams of light to be evenly distributed among the curing region, which satisfied the second purpose mentioned above.

5. Experimental Background

5.1 Relation between ICM pixels and real world dimensions

An important scaling relationship that related the pixel distance defined on the ICM video frames and the distance in the real world was based on the assumption that the ICM detecting laser beams remain collimated when transferring from the second polarizer (refer to part (6) in Figure 1) to the ICM camera (refer to part (8) in Figure 1). Following this assumption, there would be no scaling nor distortion when the ICM camera captures the light reflected from the resin chamber

(refer to the yellow lines in Figure 1) and form the ICM video frames. Thus, equation 3 was used to determine the distance in real world from the pixel distance defined on the ICM video frames:

$$D = 4 * 2.2 * d \tag{3}$$

where *D* is the distance in the real world in microns, *d* is the distance defined on the ICM video frame in pixels. The second factor *2.2* [microns/pixel] was determined from the specifications of the ICM camera which stated that both the horizontal and vertical size of a pixel of the camera was 2.2 micron [10]. The first scaling factor *4* was introduced since the ICM camera used both horizontal and vertical binning factors of 4, i.e. the camera took the average of an array of 4*4 =16 pixels to form one pixel for the ICM video frames [11]. In this case, the binning function scaled the ICM frame size ¼ time as its original size.

5.2 The Time-varying Scanning Method

The time-varying scanning method is based on the usage of the SLM. The purpose for the method is to increase the resolution of the ICM measurement in 2D dimension perpendicular to the direction of the cured part growth, without physically upgrading the experiment equipment. Figure 5 shows an example of the ICM-captured video frame, and the time-varying scanning method will be explained using this figure.

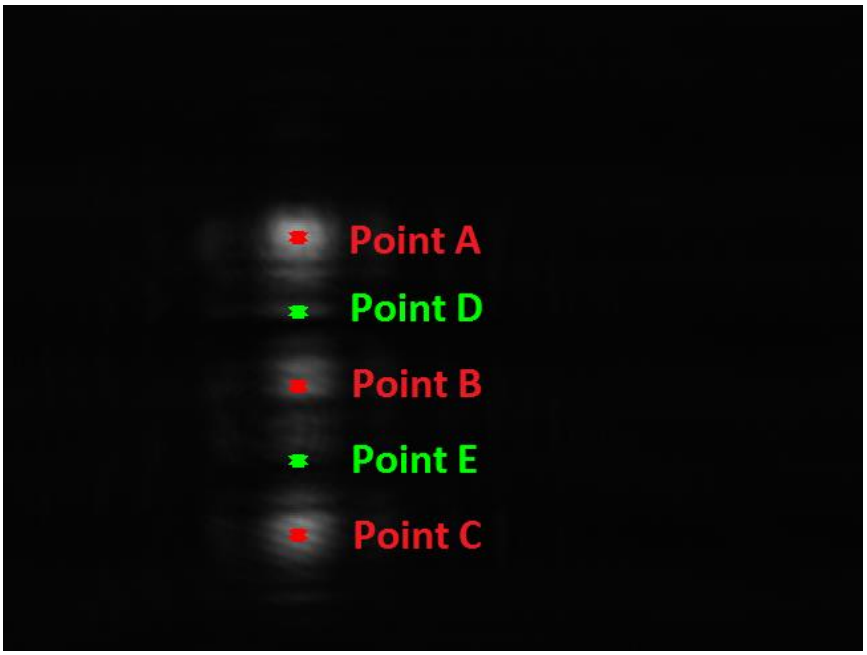

Figure 5. An example for the ICM-captured video frame

In Figure 5, the SLM was controlled to project 3 beams of ICM laser to hit the resin chamber. Three reflected light dots could be observed in this figure. Point A, B and C (the star points in red) were three points which were located at the center of the three light dot, and the interferograms at these three locations could be gathered to estimate the cured part height at these locations. The distances between point A and B and between point B and C were both 985.6

microns. Point D and E which are the green star points in Figure 5, were not intentionally lighted by the reflected ICM laser as point A, B and C did. The interferograms at point D and E could not be gathered without causing reflections of the ICM laser at these locations. However, if the SLM was controlled to have all the points A-E radiated by the ICM laser beams with the smallest beam profile achievable, the neighboring ICM laser beams (i.e. the ICM laser beam for A and D, D and B, B and E, E and C; the distances between these neighboring point pairs would all be 492.8 microns) would be too close to each other, and the internal reflections mentioned in section 4.1 would occur and would reduce the accuracy of the ICM measurement. In order to get accurate interferograms at the locations of both the green and red dots, the red points and the green points should not be illuminated by the ICM laser at the same time. Instead, only the red points will be illuminated to get their intensity values at time t; followed by only radiating the green dots at time $t+\Delta t$; then only the red points will be illuminated at time $t+2\Delta t$; then only the green points will be illuminated at time $t+3\Delta t$…… To summarize this procedure, the green and red points will be illuminated separately and their intensity values obtained (as a function of time) separately to create their corresponding interferograms. The SLM was introduced to periodically change the positions where the ICM laser beams radiate to fulfill the need for measuring the intensities at these points separately. In addition, the time gap between using the ICM laser beams to illuminate the red points set and green points set was controlled to be as small as possible so that the temporal resolution is good enough to describe the true intensity oscillations at these points. This method is called the time-varying scanning method.

6. Experimental Procedure

A series of experiments was performed to demonstrate the capability of the SLM-based ICM system to monitor the lateral extents of a curing part and the part's height distribution in real time. The experiment reported here utilized DMD images of 200x768, 250x768, 300x768, 340 x 768 and 350x768 pixels to cure a rectangular part for 24 seconds. The length of the irradiation region was approximately 4200 microns which corresponded to the 768 pixel length defined on DMD), and the width of the irradiation region approximately ranged from 1100 microns to 1900 microns which corresponded to the 200-350 pixel length range defined on the DMD. The time-varying scanning method utilized 6 sets of SLM detecting matrices. Each of these 6 detecting position sets sampled a 4x3 array of small regions, each of which was 10x10 pixels on the SLM in size (which is 88x88 microns). These regions were spaced 24 pixels apart and each column of regions was offset 6 pixels from the previous column. These regions were defined to let the ICM detecting beam pass through the SLM. Within each period of running these 6 SLM detecting matrix sets, the difference between two neighboring SLM position sets was that the second position set was offset 1 pixel (defined on the SLM) from the previous position set, which resulted in 5 pixel (defined on the ICM camera) difference in the ICM measurement. Plugging this 5 pixel difference into equation (3), it could be found that the resolution of the ICM measurement was 44 microns. In addition, when the SLM was controlled to display these 6 SLM detecting matrix sets, there was also an additional 10x10 pixel region opened on the SLM which was called the SLM frame indicator. The position of the SLM frame indicator was unique for each of the 6 SLM detecting matrix sets. These unique positions were used to indicate which of the 6 SLM detecting matrix sets the current ICM video frame corresponded to. It is important to know the corresponding SLM detecting matrix set mentioned above, since for each of the SLM detecting matrix sets (which was 4x3 array of small regions) there was also a unique corresponding set of 4x3 point-positions

defined on the ICM video frame which was called the ICM detecting positions. These ICM detecting positions were pre-calibrated before the experiment so that the ICM detecting position sit at the center of the corresponding reflected light from the 10x10 opened positions (the SLM detecting matrix) on the SLM. The grayscale intensity values (out of 255) at the ICM detecting positions were recorded to create the interferograms at those locations. Since there were 6 sets of 4x3 SLM detecting matrices, it corresponded to 6 sets of 4x3 ICM detecting positions which had 72 detecting positions in total.

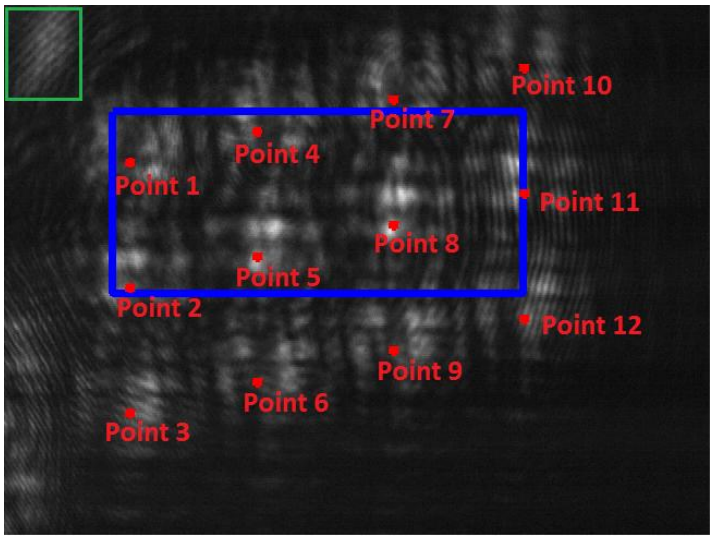

Figure 6. First set of ICM detecting locations on the ICM video

Figure 6 shows the ICM video frame in which light was gathered from the reflected ICM laser from the first SLM detecting matrix set. In addition, the first set of ICM detecting positions was indicated by the red points 1-12. The intensity values at these 12 locations will be recorded to generate the interferograms at these locations. The green rectangle indicates that the SLM frame indicator for the first set of the SLM detecting matrix was located at the top-left corner of the ICM video frame where the intensity is higher than the black background. The blue rectangle indicates the UV radiation region on the ICM video frame.

Figures 7, 8, 9, 10, 11 show the other 5 typical ICM video frames, and each of them corresponds to the other 5 SLM detecting matrix sets (i.e. the other 5 sets of 4x3 arrays of 10x10 small regions opened on the SLM) and their corresponding SLM frame indicators. Similarly, these 5 figures also correspond to the 5 sets of ICM detecting positions indicated by the red points. Figure 12 plots all the 6 ICM detecting position sets on one ICM video frame with the blue rectangle indicating the irradiated region during that experiment, with the SLM fully-opened for that frame.

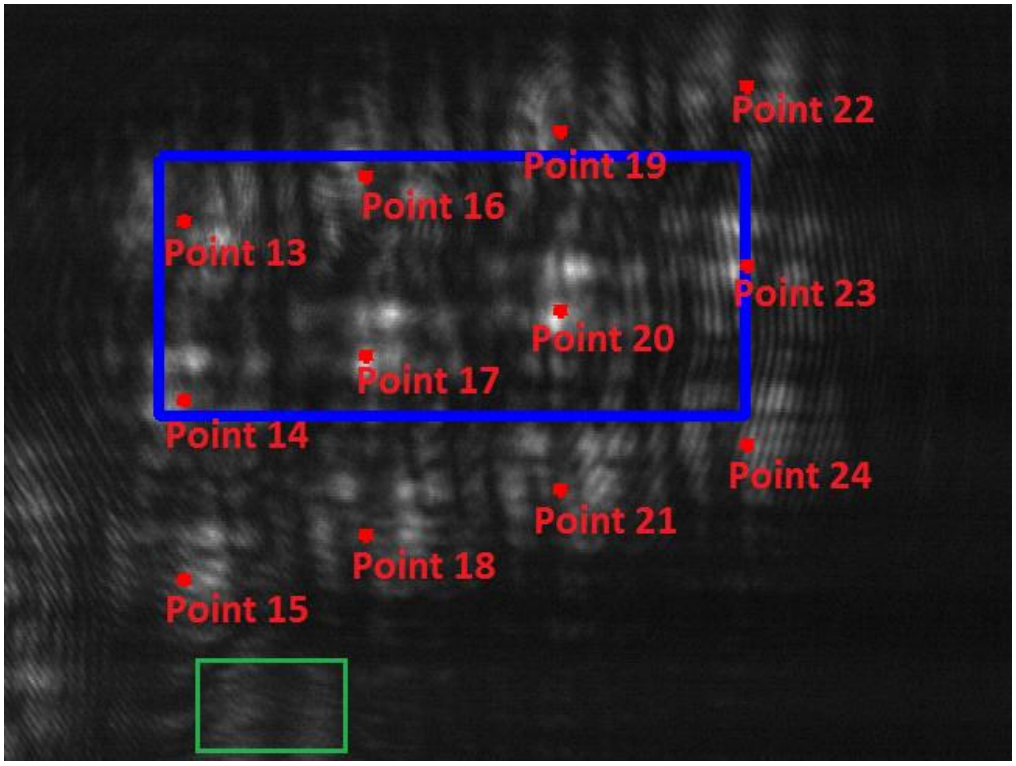

Figure 7. Second set of ICM detecting locations on the ICM video

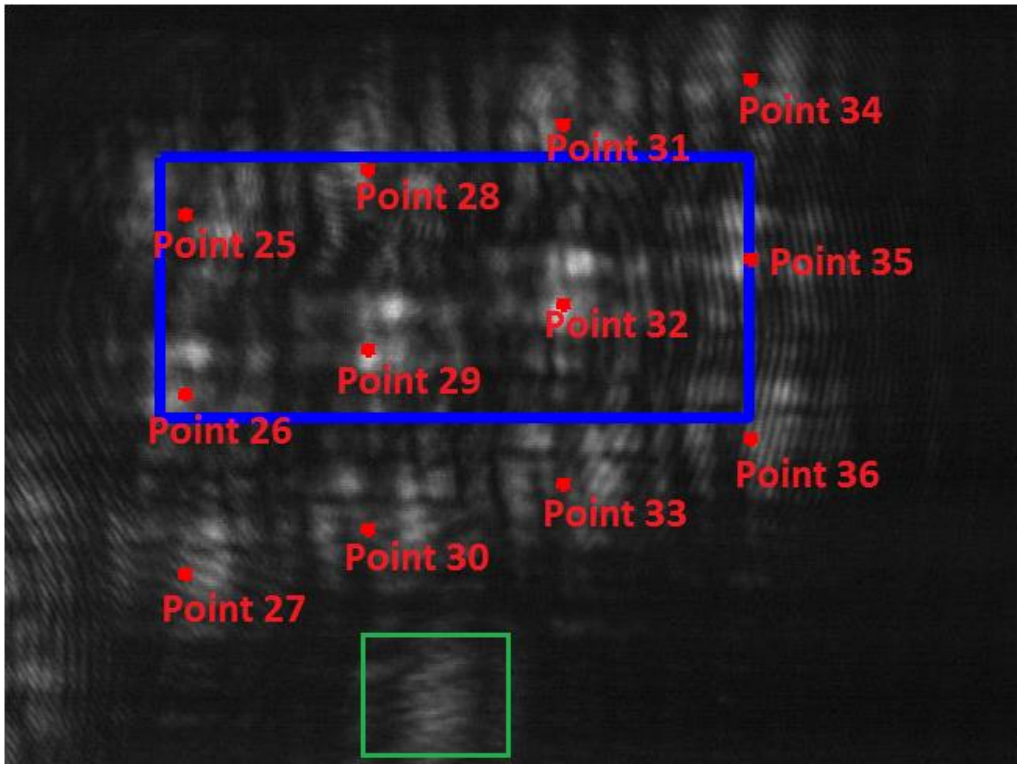

Figure 8. Third set of ICM detecting locations on the ICM video

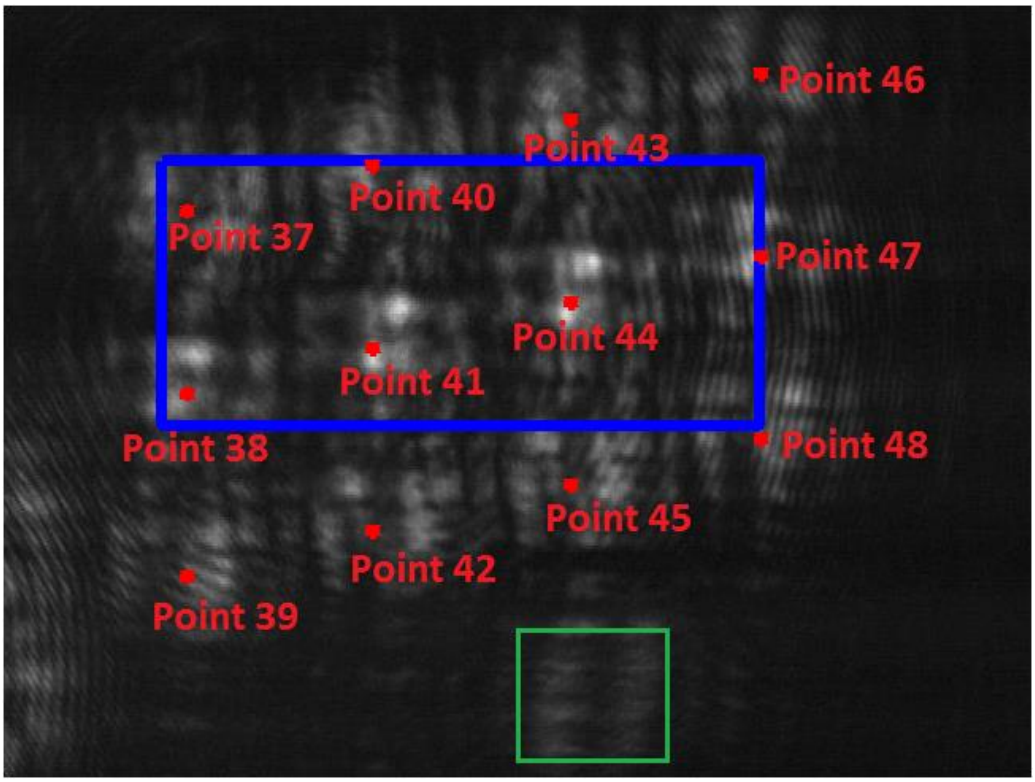

Figure 9. Fourth set of ICM detecting locations on the ICM video

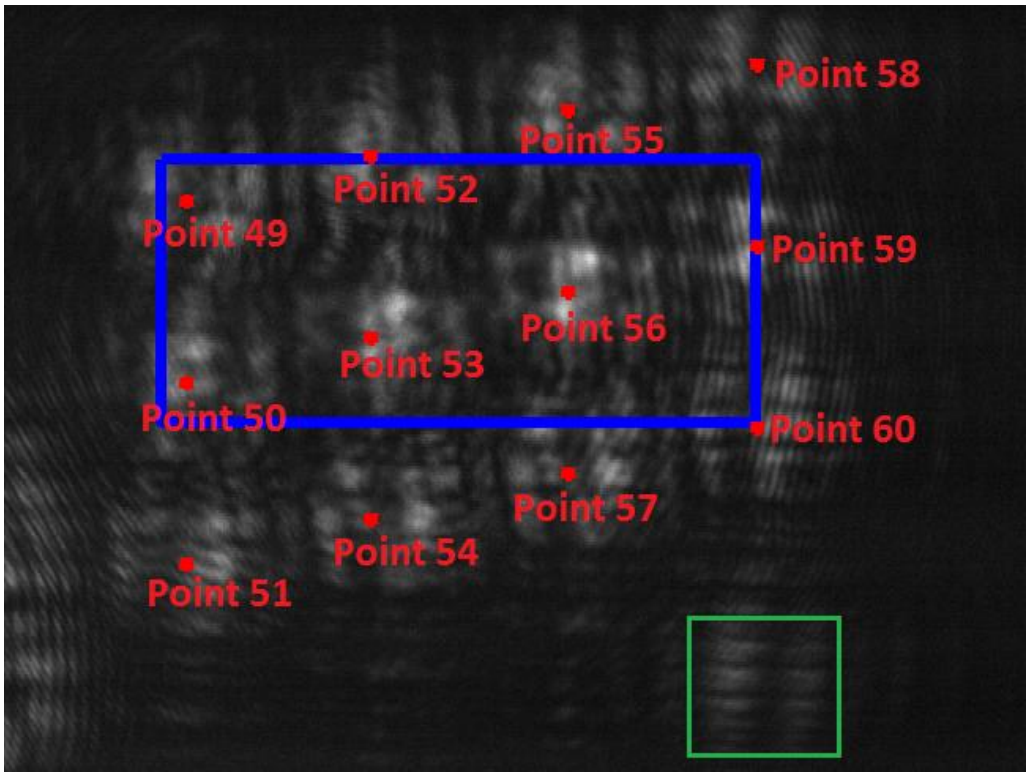

Figure 10. Fifth set of ICM detecting locations on the ICM video

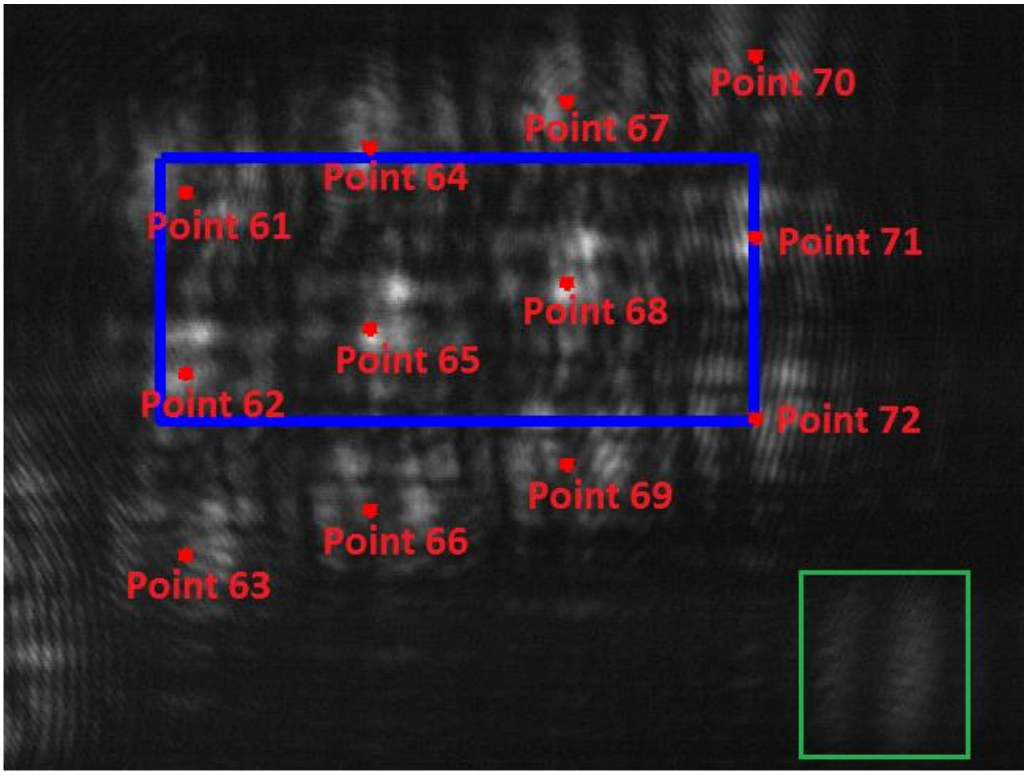

Figure 11. Sixth set of ICM detecting locations on the ICM video

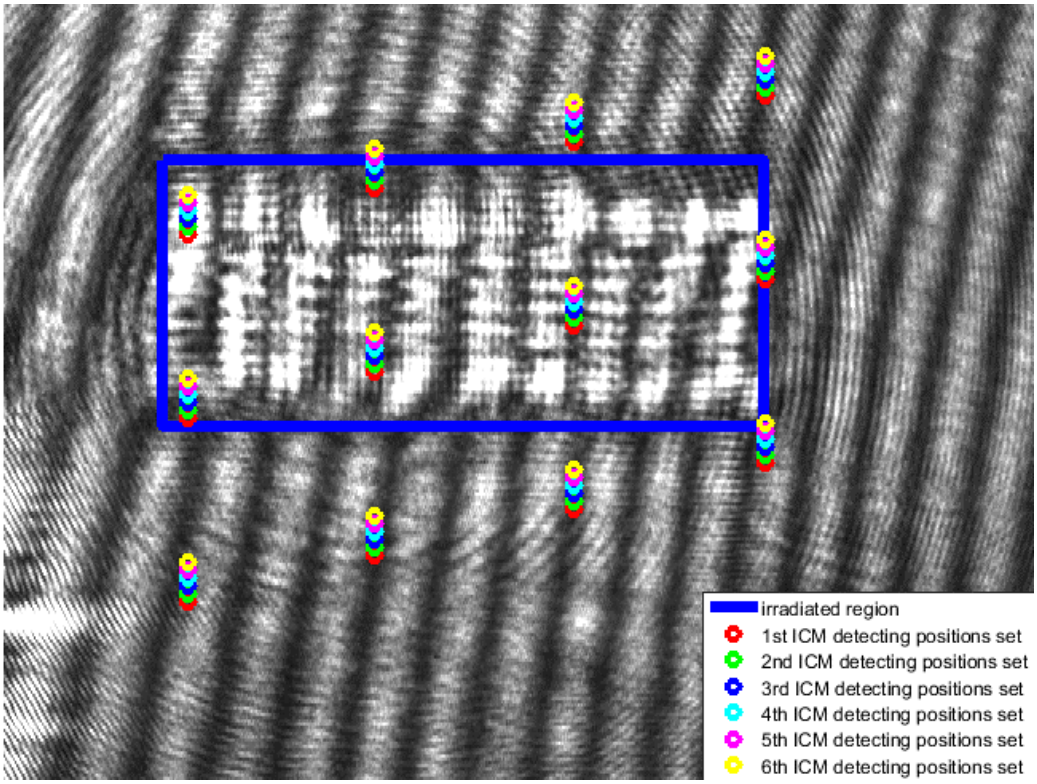

Figure 12. All the ICM detecting positions plotting on one ICM video frame

The ICM measuring process was taken throughout the whole ECPL curing process. During the ICM measuring process, the 6 sets of SLM detecting matrices, i.e. the 6 sets of 4x3 array of 10x10 pixel (defined on SLM) regions opened on the SLM, was periodically shown on the SLM. The time step for each SLM detecting matrix set to be displayed on the SLM was 0.03 second. The ICM camera was used to capture the light reflected from the resin chamber which is the yellow line on Figure 1. The frame rate for the ICM-captured video was set as 35 Hz. After the ICM camera capture the ICM video for the whole curing process, it was analyzed to get the interferograms at each of the SLM detecting matrices. There was an identification process, consisting of two steps, before analyzing each of the ICM video frames: 1) The first step was, for each frame in the ICM video, the frame was defined as "functional" if and only if it contains only one of the six sets of SLM detecting matrices; this evaluation was achieved by identifying if only one of the six SLM frame indicators showed reflected light (that reached a pre-calibrated threshold light intensity) in each ICM video frame. 2) The second step was, for each frame in the ICM video, after the frame was identified to be "functional", the SLM frame indicator position was used to identify which ICM detecting position set was illuminated. For each ICM video frame that passed the 2-step identification process, the intensity values (out of 255) at the corresponding ICM detecting positions, associated with the time step information of that ICM video frame, were stored to create the intensity vs time plots, which were the interferograms for each detecting positions.

It was expected that interferograms recorded at sampled points within the irradiated region (points 1, 2, 4, 5, 8, 11, 13, 14, 16, 17, 20, 23, 25, 26, 28, 29, 32, 35, 37, 38, 41, 44, 47, 49, 50, 53, 56, 59, 61, 62, 65, 68, and 71) would indicate significant curing, while at sampled points outside of the irradiated region (points 3, 6, 9, 10, 12, 15, 18, 19, 21, 22, 24, 27, 30, 31, 33, 34, 36, 39, 42, 43, 45, 46, 51, 54, 55, 57, 58, 63, 66, 67, 69, and 70), no curing would be indicated. As an indication of curing, an interferogram will have well defined and large amplitude oscillations. At other points, interferograms with small amplitude or random oscillations might be observed. In addition, it was assumed that the upper and lower horizontal edges of the cured part were parallel to the upper and lower edges of the ICM video frames.

7. Results and Discussion

The interferograms were analyzed, and the total phase shift and average amplitude of the intensity oscillations at each monitored positions were recorded. Figure 13 shows the interferograms recorded at sampled points 20, 28, and 30. Coinciding with the expectation, the interferogram from point 20 had large amplitude oscillations, while at point 30 the interferogram was flat. At point 28 which is close to the edge of the irradiated region, oscillations with much smaller amplitudes were observed.

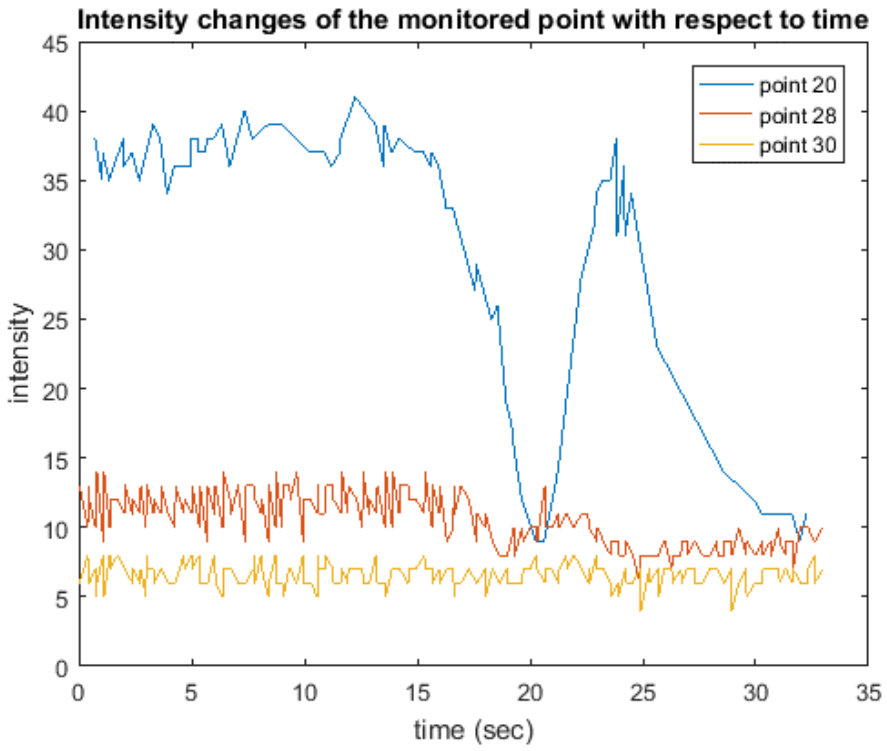

Figure 13. Interferograms at point 20, 28, and 30

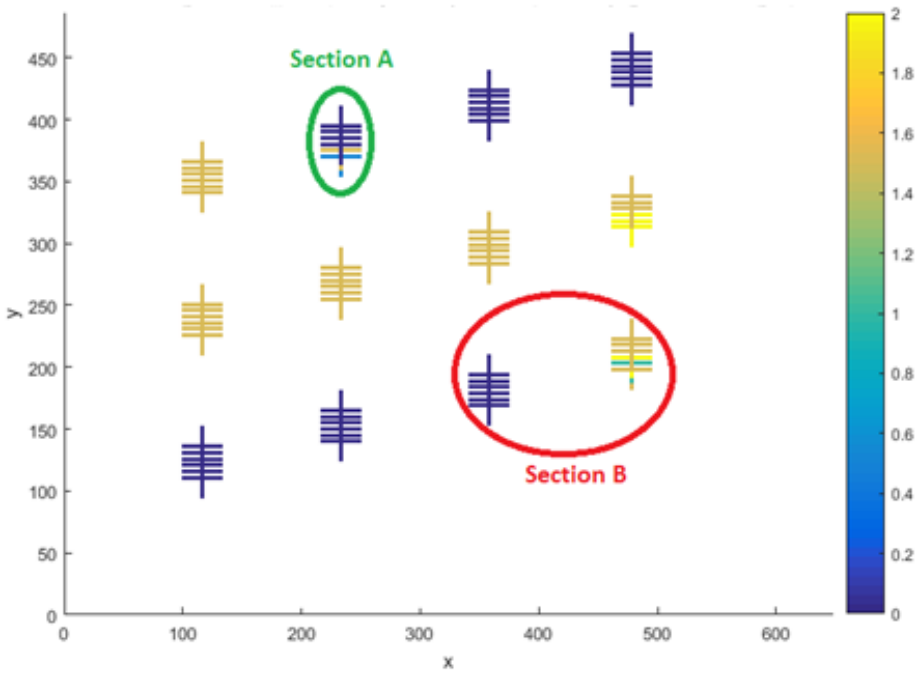

Figure 14. Resultant number of oscillation periods among the monitored points

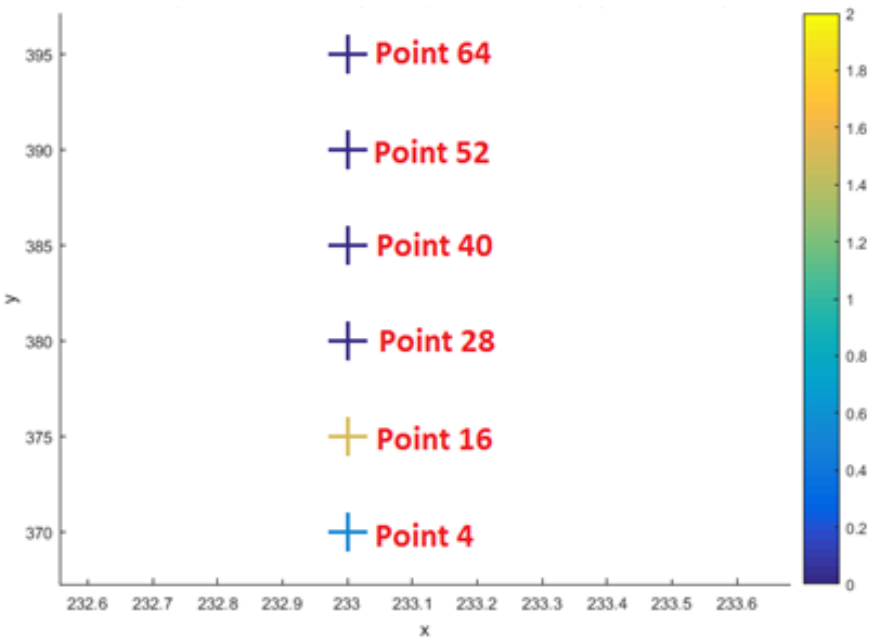

Figure 15. Zoomed in view of Figure 14 for the section A

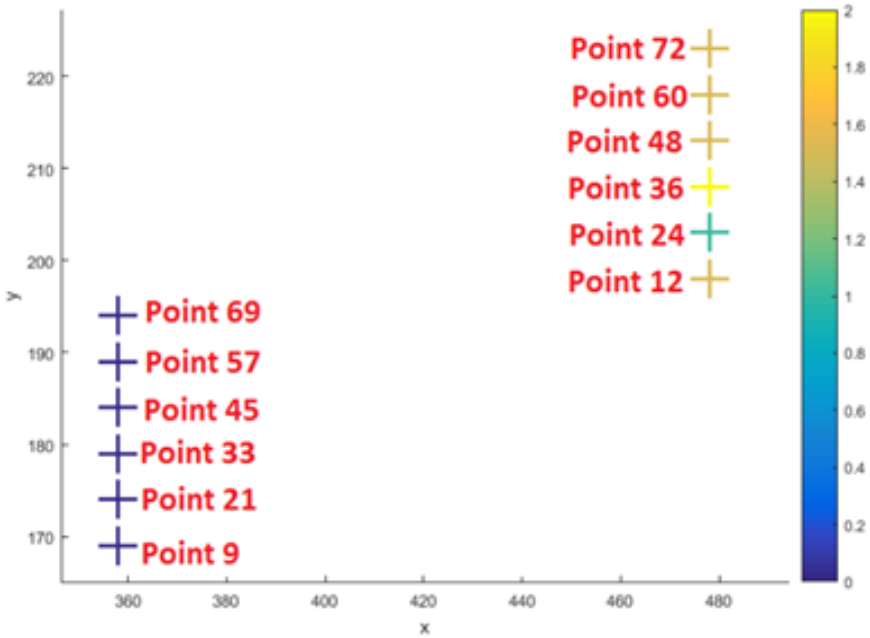

Figure 16. Zoomed in view of Figure 14 for the section B

As an example, Figure 14 shows the resultant number of intensity oscillation periods at each monitored point for an experiment that used the DMD image of 340 x 768 pixels to cure a rectangular part for 24 seconds. Figures 15 and 16 show the zoomed in view of Figure 14 at section A and B. In Figure 14, the number of oscillations at each ICM detecting position is indicated in a 2D layout where the number of oscillations was indicated by the color bar on the right. Each cross-mark indicates one ICM detecting position. This plot helped determine the 1D vertical dimension (i.e. the width) of the cured part. From Figure 15, since point 28 had 1.5 oscillation periods while

point 40 did not have any oscillation periods, it could be concluded that the top edge of the curing region was located between point 28 and point 40. Similarly, from Figure 16, point 12 had 1.5 oscillation periods while point 69 did not have any oscillation periods, it could be concluded that the bottom edge was between point 12 and point 69. The width of the cured part should be defined by the distance between the top and bottom edges of the curing region. Using equation 3 in section 5.1, it was determined that the vertical width of this cured part was approximately 1600 microns. On the other hand, the measurement from microscope indicated that the width of this cured part was 1860 microns. Table 1 shows more experiment results with different sizes of the irradiation region defined by pixel lengths on the DMD. Note that the percentage difference was calculated using Equation 4

$$Percentage\ Difference = \frac{(ICM)-(Microscope)}{(Microscope)} * 100\% \quad (4)$$

where *(ICM)* stands for the width measurement from the time-varying ICM scanning method, and *(Microscope)* stands for the width measurement from the microscope. Four reasons could explain the difference between the ICM measurements and the microscope measurements. Firstly, this difference consisted of the theoretical resolution of the ICM measurement which was 44 microns. Secondly, the deviations of the results could come from the errors of the microscope measurement. When defining the edges of the cured part on the microscope, there could be a manual error of ±30 microns for each edge. Thirdly, the edges of the fabricated parts were not walls that were perfectly perpendicular to the substrate glass slides, but some slanted walls. This caused the height distribution near the edges to be a transition from the desired height of the fabricated part to zero in height, which made the edge fuzzy to be observed by the ICM. This fuzzy edge zone could contribute to ±40 microns to the deviation between the ICM measurements and the microscope measurements. Fourthly, imperceptible damage during the washing process could be an explanation for the difference between the ICM measurements and the microscope measurements. These damage could contribute to an error of ±32 microns. So that total error can be ± 146 microns.

Table 1. Estimated and Measured Part Widths

Irradiation Size Defined by DMD pixel length	Width in [μm] From ICM	Width in [μm] From Microscope	Difference in [μm]	Percentage difference in %
200x768	1012.0	1075	-63.0	-6%
210x768	1012.0	1135	-123.5	11%
220x768	1091.2	1194	-102.6	-9%
230x768	1135.2	1248	-112.5	-9%
240x768	1179.2	1306	-126.8	-10%
250x768	1267.2	1399	-131.7	-9%
260x768	1267.2	1437	-169.9	-12%
270x768	1311.2	1470	-158.7	-11%

Table 1 (Continued). Estimated and Measured Part Widths

Irradiation Size Defined by DMD pixel length	Width in [μm] From ICM	Width in [μm] From Microscope	Difference in [μm]	Percentage difference in %
280x768	1412.4	1529	-116.9	-8%
290x768	1496.0	1583	-87.5	-6%
300x768	1438.8	1624	-184.8	-11%
310x768	1474.0	1704	-230.4	-14%
320x768	1601.6	1770	-168.1	-10%
330x768	1768.8	1801	-31.8	-2%
340x768	1597.2	1860	-262.7	-14%
350x768	1808.4	1927	-118.3	-6%

In addition to the lateral width, the height distribution of the cure part can also be estimated. From previous work [13], a linear relationship is expected between the natural logarithm of the phase angle and the cured part height. The relative height of the cured part at each ICM monitored position could also be found based on the expected linear relationship.

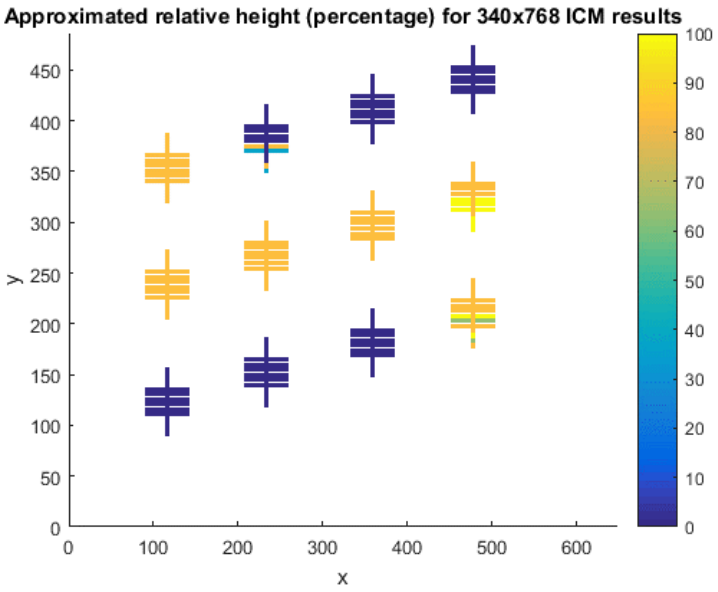

Figure 17. Relative height (percentage of the maximum height) distribution of the cured part defined by 340x768 DMD radiation region size

Figure 17 shows the relative height distribution of the cured part sample described in Figure 14. The relative height was defined as the percentage of the maximum height found within that cured part by the ICM scanning method. The height distribution agreed with the part height measurements taken with a confocal microscope. Future work needs to be done to determine the parameters in the expected linear relationship.

8. CONCLUSIONS

This paper presented a method to measure 1D lateral dimensions and the relative height distribution of cured parts during the ECPL curing process, based on a time-varying multi-point monitoring method with the ICM system. The main conclusions are listed as follows:

1. Using a matrix of ICM detecting laser beams that are sampled sequentially, the width of the cured part could be efficiently measured.

2. The ICM detecting resolution in 2D lateral directions (perpendicular to the direction of the growth of the cured part) could be successfully improved, without physically upgrading the equipment, by introducing time variance in addition to the 2D spatial dimensions.

The parameters within the expected linear relationship between the natural logarithm of the number of intensity oscillation periods and the height of the cured part (i.e. equation 2) needs to be investigated so that the height distribution of the cured part could be described more accurately. In addition, to further improve the ICM detecting resolution in the 2D lateral directions, a beam expander similar to part (2) in Figure 1 could be inversely introduced after the second polarizer (part (6) in Figure 1) in order to shrink the gap between two neighboring ICM detecting laser beams without making them interfere with each other. The feasibility of this method could be investigated as future work to further improve the resolution of the ICM method.

9. ACKNOWLEDGMENTS

This material is based upon work supported by the National Science Foundation under Grant No. CMMI-1234561. Any opinions, findings, and conclusions or recommendations expressed in this publication are those of the authors and do not necessarily reflect the views of the National Science Foundation. All the related research is patent pending.

The work related to the confocal microscope was performed in part at the Georgia Tech Institute for Electronics and Nanotechnology, a member of the National Nanotechnology Coordinated Infrastructure, which is supported by the National Science Foundation (Grant ECCS-1542174).

10. Reference

[1] Limaye A., Rosen D., 2007, "Process Planning Method for Mask Projection Micro-Stereolithography", *Rapid Prototyping Journal*, 13(2), pp. 76-84.
[2] Sun C., Fang N., Wu D.M., Zhang X., 2005, "Projection Micro-Stereolithography Using Digital Micro-Mirror Dynamic Mask", *Sensors and Actuators A,* 121, pp. 113-120.
[3] Chatwin C., Farsari M., Huang S., Heywood M., Birch P., Young R., Richardson J., 1998, "UV Microstereolithography System That Uses Spatial Light Modulator Technology", *Applied Optics*, 37(32), pp. 7514-22.
[4] Monneret S., Loubere V., Corbel S., 1999, "Microstereolithography Using Dynamic Mask Generator and A Non-Coherent Visible Light Source", *Proc. SPIE,* 3680, pp. 553-561.
[5] Jariwala A., Ding F., Zhao X., Rosen D., 2009, "A Process Planning Method for Thin Film

[6] Zheng X., Deotte J., Alonso M.P., Farquar G.R., Weisgraber T.H., Gemberling S., Lee H., Fang N., Spadaccini C.M. "Design and optimization of a light-emitting diode projection micro-stereolithography three-dimensional manufacturing system."*Review of Scientific Instruments* 83.12 (2012): 125001.
[7] Jariwala A., Ding F., Zhao X., Rosen D., 2008, "A Film Fabrication Process on Transparent Substrate Using Mask Projection Stereolithography", D. Bourell, R. Crawford, C. Seepersad, J. Beaman, H. Marcus, eds., *19th SFF Symp.*, Austin, Texas, pp. 216-229.
[8] Jariwala A., Ding F., Boddapati A., Breedveld V., Grover M. A., Henderson C. L., Rosen D. W., 2011, "Modeling effects of oxygen inhibition in mask-based Stereolithography", *Rapid Prototyping Journal*, 17(3), pp. 168-175.
[9] Schwerzel R.E., Jariwala A.S., Rosen D.W., 2013, "A Simple, Inexpensive, Real-Time Interferometric Cure Monitoring System for Optically Cured Polymers," *J. Applied Polymer Science*, Vol. 129, No. 5, pp 2653-2662.
[10] "AcA2500-14gm Specifications." Basler AG, 2016. Web. Accessed 15 July 2016. http://www.baslerweb.com/en/products/cameras/area-scan-cameras/ace/aca2500-14gm
[11] Basler Ace USER'S MANUAL FOR GigE CAMERAS. Exton: Basler, 2016. AcA2500-14gm. Basler, Inc., 01 June 2016. Sec. 8.13. Web. Accessed 15 July 2016. http://s.baslerweb.com/media/documents/AW00089323000_ace%20GigE%20Users%20Manual.pdf
[12] Jones H.H., Kwatra A., Jariwala A.S., Rosen D.W. "Real-time selective monitoring of exposure controlled projection lithography." *Proceedings of the 24th Solid Freeform Fabrication Symposium*. 2013.
[13] Jones H.H., Jariwala A.S., Rosen D.W., 2014, "Towards Real Time Control of Exposure Controlled Projection Lithography," *International Symposium on Flexible Automation*., Awaji Island, Japan, July 14-16.